Measurements of Counter Flow Region in Averaged Wake-Velocity-Field of a Small Straight-Bladed Vertical Axis Wind Turbine

Yutaka Hara[1]
Takahiro Suzuki[1]
Hirofumi Kamon[2]

[1]Department of Mechanical and Aerospace Engineering, Graduate School of Engineering
Tottori University
Koyama-cho, Tottori 680-8552
Japan
hara@damp.tottori-u.ac.jp

[2]Department of Applied Mathematics and Physics, Faculty of Engineering
Tottori University

Abstract

To determine the three-dimensional flow field around vertical axis wind turbines (VAWTs), an ultrasonic anemometer was used to measure the three components of flow velocity in the wake of a small VAWT (4-blade rotor; airfoil: NACA 0012; rotor diameter: 0.6 m; blade length: 0.47 m; chord length: 0.075 m). Counterflow in the direction of the mainstream was observed even in the averaged wake-flow field. For a more detailed investigation of the counterflow regions, the three-dimensional flow field was reconstructed through computation from the velocity data obtained at each measurement point and was analyzed by means of velocity vector maps, vorticity distributions, and path lines. A clear swirl pattern in two-dimensional path lines was observed near the counterflow region on the equatorial plane in the wake; however, the vorticity of the swirl pattern part was weak.

Key words: wind turbine, wake, VAWT, counterflow

Introduction

Research and development of various types of vertical axis wind turbines (VAWTs) has been conducted, focusing on the characteristic of being unaffected wind direction variations. Although calculations based on blade element momentum (BEM) theory [1-3] are generally useful for designing and evaluating the performance of wind turbines, in the case of small and micro wind turbines, the lack of high-precision aerodynamic data at low Reynolds number [4], the dynamic stall effect [1], and other factors have a large impact that makes it difficult to model experimental values with high precision. Gaining a three-dimensional understanding of the flow field around a wind turbine is considered important for improving the precision of BEM calculation of small VAWTs. An ultrasonic anemometer has previously been used to measure a particular cross section of VAWT wake, and these measurements have indicated the existence of a counterflow region in the averaged flow field [5-7].

In this research, velocity measurements were performed in many more cross sections, in addition to the particular cross section that was previously measured, in order to understand the details of the VAWT wake that produces the counterflow region. The three-dimensional averaged flow field was reconstructed by merging the obtained velocity data through computation. Details of the averaged flow field in the vicinity of the counterflow region observed in the VAWT wake were clarified by rendering information such as velocity vector maps, vorticity distribution, and flow paths of arbitrary cross sections of the obtained averaged flow field to analyze the flow from various perspectives.

Nomenclature

c: Blade chord length (m)
C_p: Power coefficient (Eq. (1))
C_q: Torque coefficient (Eq. (2))
D: Rotor diameter (m)
H: Rotor height (blade span length) (m)
N: Rotation speed (min^{-1})
P: Power (W)
Q: Torque (Nm)
R: Rotor radius (m)
Re_b: Blade Reynolds number ($V_{rel}\, c / \nu$)
U, V, W: Velocity components (m s^{-1})
U_0: Upstream uniform velocity (m s^{-1})
V_{rel}: Relative velocity (m s^{-1})
X, Y, Z: Position coordinates (m)
λ: Tip-speed ratio ($R\omega/U_0$)
ν: Coefficient of kinematic viscosity (m^2 s^{-1})
ρ: Air density (kg m^{-3})
ω: Angular velocity (rad s^{-1})

Experimental Apparatus and Methods

Figure 1 shows a schematic diagram of the experimental apparatus, and Fig. 2 shows a photograph of the experimental wind turbine as viewed from the downstream side. A straight-bladed vertical axis wind turbine employing the NACA 0012 airfoil (c = 0.075 m) was used in this research. The number of blades was 4, the rotor diameter was D = 0.6 m, and the rotor height was H = 0.47 m. The wind turbine rotation axis was located at a position 1.5 m downstream from the wind tunnel nozzle (1.5 × 1.5 m). The rotor was connected to an induction motor via a torque detector, and was made to rotate at a particular fixed rotation speed by an inverter. An ultrasonic anemometer was used for measurements. The coordinate system and range of measurements are shown in Fig. 3. Constant velocities of 5 and 10 m s^{-1} were generated in the wind tunnel, and the three velocity components (U, V, and W) were measured at 10 cross sections perpendicular to the main flow at positions in the range of 0.6 m ≤ X ≤ 1.5 m downstream from the rotor center. The range of measurements in the direction perpendicular to the main flow was -0.6 m ≤ Y ≤ 0.6 m and -0.5 m ≤ Z ≤ 0.6 m, and the measurement points were spaced at intervals of 0.1 m along each of the Y axis and Z axis directions. The sampling frequency of the ultrasonic anemometer was 32 Hz, with approximately 1240 pieces of data (duration of approximately 40 s) acquired at each measurement point.

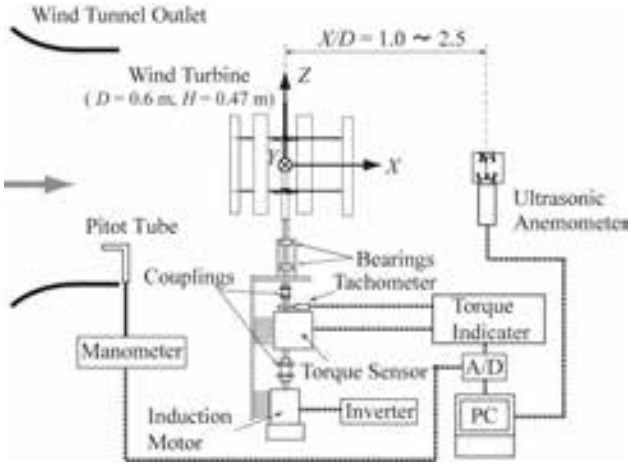

Fig. 1 Schematic of experimental system

Fig. 2 Photograph of experimental apparatus

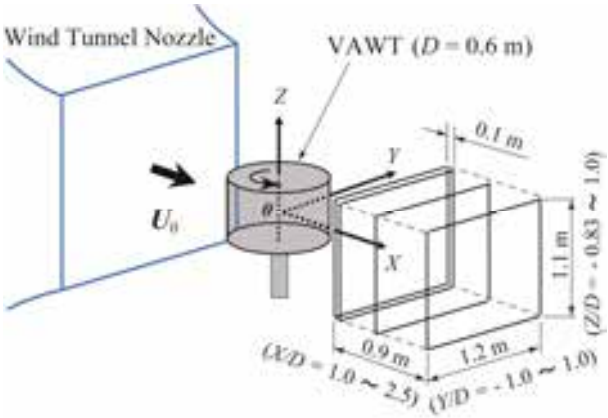

Fig. 3 Coordinate system and measurement domain

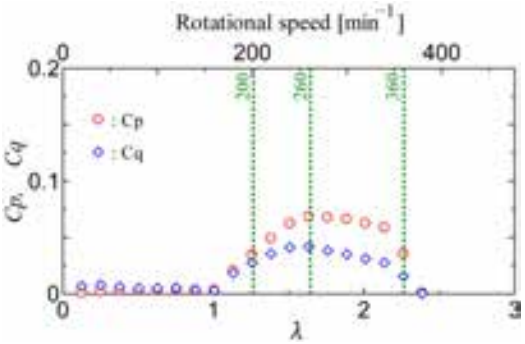

Fig. 4 Power and torque characteristics of experimental VAWT at U_0 = 5 m s^{-1}

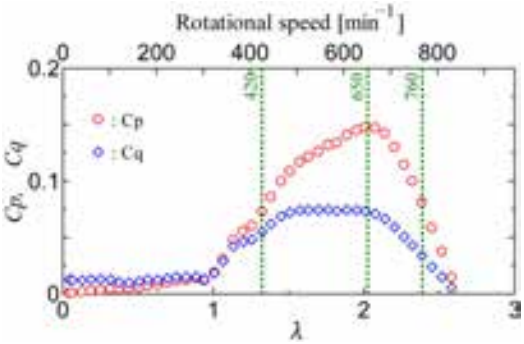

Fig. 5 Power and torque characteristics of experimental VAWT at U_0 = 10 m s^{-1}

Figures 4 and 5 show the power coefficient (C_p) and torque coefficient (C_q) versus the tip-speed ratio (λ) at each of the wind velocities of 5 and 10 m s^{-1} at which the VAWT was evaluated in this research. The equations defining the power coefficient and torque coefficient are shown in Eqs. (1) and (2), where P is the wind turbine power, Q is the torque, and ρ is the air density.

$$C_p = \frac{P}{0.5\rho U_0{}^3 (DH)} \tag{1}$$

$$C_q = \frac{Q}{0.5\rho U_0{}^2 (DH)R} \tag{2}$$

Experiments were conducted under three conditions: the condition where the rotation speed equals the maximum efficiency point of the wind turbine; a low rotation speed condition where the power is 50% of the maximum efficiency point; and a high rotation speed condition. More specifically, for U_o = 5 m s^{-1}, the rotation speeds were 200, 260, and 360 min^{-1}, and for U_o = 10 m s^{-1}, the rotation speeds were 420, 650, and 760 min^{-1}. The Reynolds number of the blade based on the blade chord length Re_b at the maximum efficiency point is approximately 4×10^4 at U_o = 5 m s^{-1} and approximately 1×10^5 at U_o = 10 m s^{-1}.

Experimental Results and Discussion

Figure 6 shows the distribution of the U velocity component at the equatorial plane (Z/D = 0) for the case of wind velocity U_o = 10 m s^{-1} and rotation speed N = 650 min^{-1}. The area of filled circles is the counterflow area. Figure 7 shows a three-dimensional volume rendering of the counterflow region in this same state. The white solid line in Fig. 7 indicates the measurement range. The wind turbine rotates in the counterclockwise direction when viewed from above. From Figs. 6 and 7, the counterflow region exists centered at a position shifted slightly above and on the right side of the center as viewed from the downstream side.

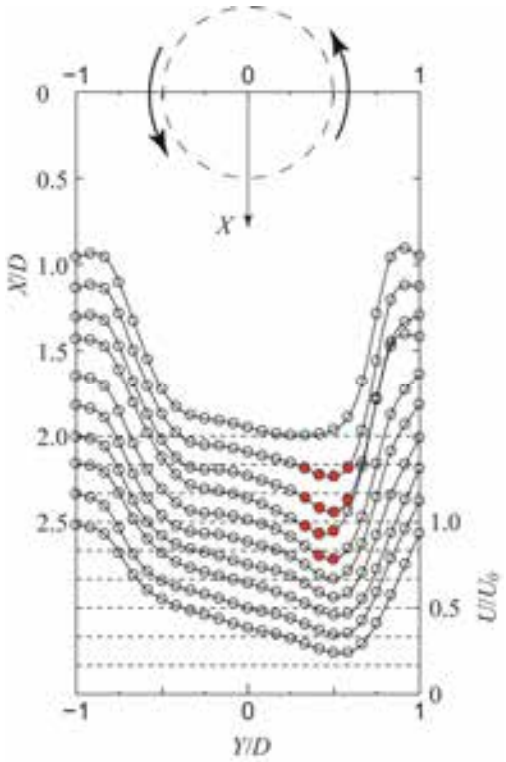

Fig. 6 Distributions of velocity component *U* on equatorial plane in wake (U_0 = 10 m s^{-1}, N = 650 min^{-1})

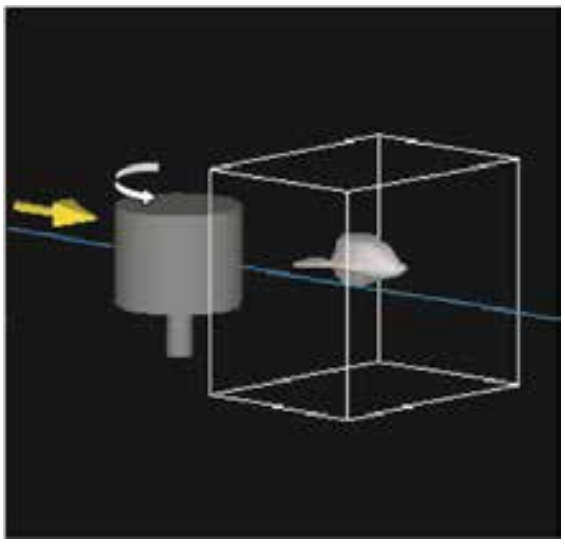

Fig. 7 Volume rendering of counterflow region (U_0 = 10 m s^{-1}, N = 650 min^{-1})

Figure 8 shows the distribution of the U velocity component versus rotor rotation speed in the Y-Z plane at the position X/D = 1.5 for the case of U_0 = 10 m s^{-1}. The dotted line in the figure shows the outline of the wind turbine and central support pillar. The blade near Y/D = 0.5 on the right side of the center in Fig. 8 is moving in the reverse direction to the main flow while the blade near Y/D = -0.5 on the left side of the center is moving in the same direction as the main flow. Although Fig. 8(c) shows that a counterflow region was observed in the wake region at the right edge of the rotor (near Y/D = 0.5), a counterflow region has also been observed in the wake region at the left edge of the rotor (near Y/D = -0.4) further upstream from X/D = 1.17 under the same rotation speed conditions [7]. Although Fig. 8 shows the case for the high wind velocity (U_0 = 10 m s^{-1}), since the wind velocity distribution patterns were the same at the low wind velocity (U_0 = 5 m s^{-1}), only the results for the high wind velocity are shown in this paper. Furthermore, we focus our discussion on the counterflow region in the maximum power state (N = 650 min^{-1}). The results presented subsequently are therefore all results for the averaged flow field in the U_0 = 10 m s^{-1} and N = 650 min^{-1} state.

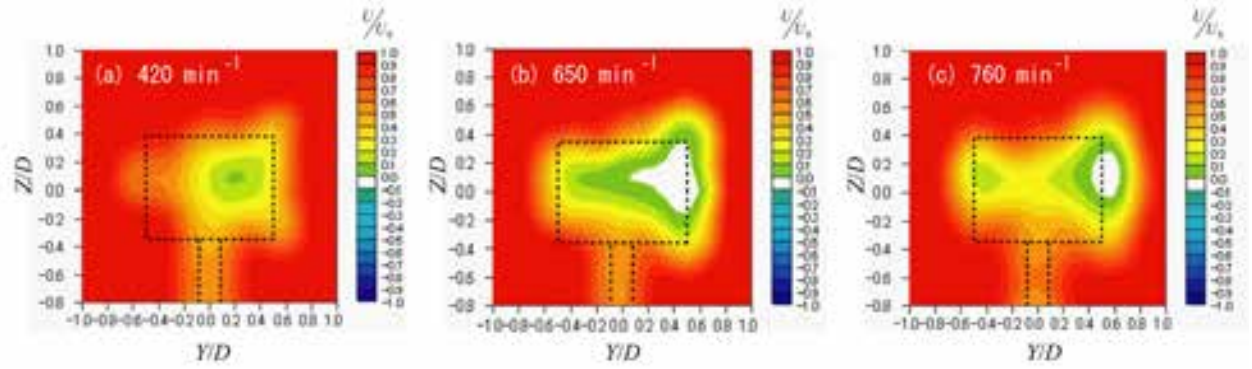

Fig. 8 Distributions of velocity component *U* on vertical plane of X/D = 1.5 (U_0 = 10 m s^{-1})

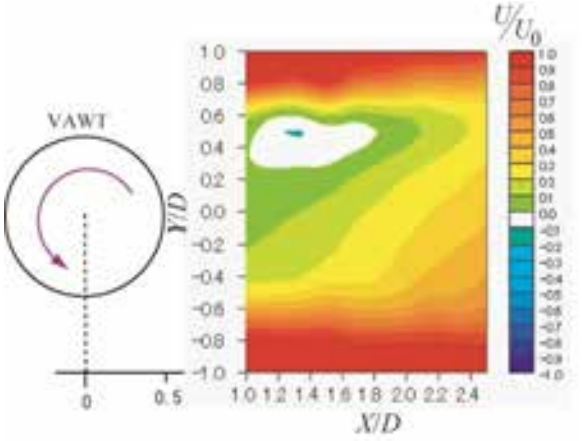

Fig. 9 Distribution of velocity component *U* on equatorial plane

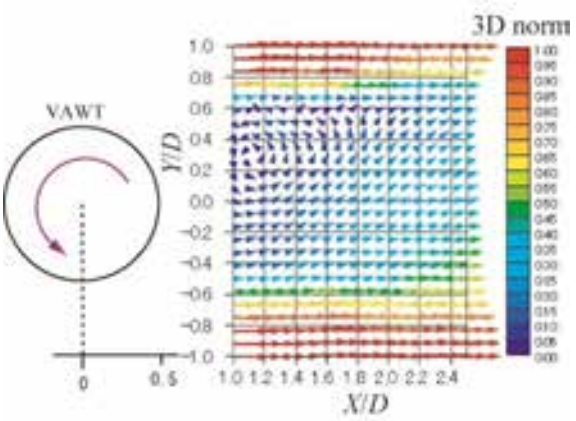

Fig. 10 Two-dimensional velocity vector map on equatorial plane

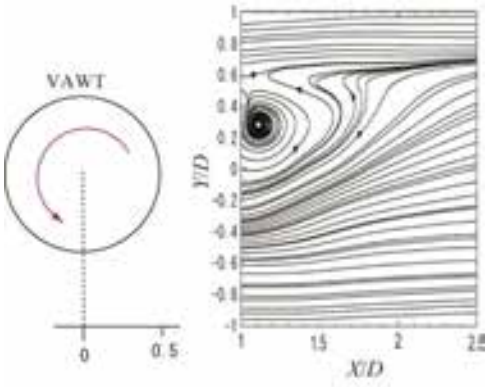

Fig. 11 Two-dimensional path lines on equatorial plane

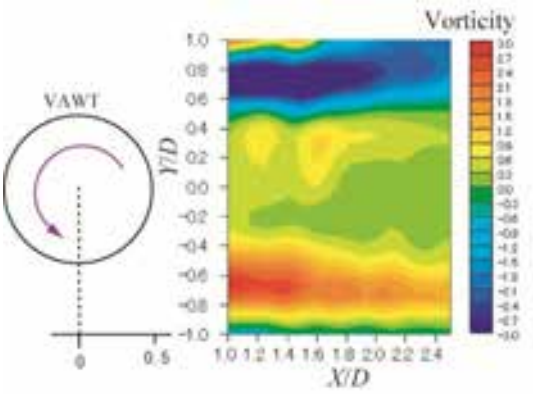

Fig. 12 Distribution of vorticity on equatorial plane

Figure 9 shows the distribution of the *U* velocity component at the equatorial plane ($Z/D = 0$) for the case of $U_0 = 10$ m s^{-1} using contour lines (i.e., a different representation of Fig. 6). The direction of the main flow is from left to right in the figure. According to Fig. 9, the region where counterflow exists in the equatorial plane gradually shrinks further downstream until it ceases to exist near $X/D = 1.8$.

Figures 10 to 12 show the two-dimensional velocity vector map (*U*, *V*), two-dimensional flow path lines, and vorticity distribution under the same conditions and at the same cross section as Fig. 9. Note that the color density of the vectors in Fig. 10 indicates the magnitude of the three-dimensional velocity vectors normalized by the main flow velocity in dimensionless units. A counterclockwise rotating vortex flow pattern (centered at $X/D = 1.1$, $Y/D = 0.3$) can be observed near the counterflow region in Figs. 10 to 12, and it is clear that the counterflow region in the *U* velocity component is generated by the drag into this vortex. However, as shown in the vorticity distribution in Fig. 12, the vorticity of the vortex pattern that is clearly observed in Fig. 11 does not exhibit a significantly higher value than the surroundings.

Figures 13 and 14 show the distribution of the *U* velocity component and the two-dimensional flow path lines in the *X*-*Z* vertical cross section at the position $Y/D = 0.5$. At this position, the counterflow region spreads out in the vertical direction (*Z* direction) and the flow path lines exhibit complex flow patterns. Although a pair of vertically aligned vortexes appears to exist by cursory inspection, the vorticity at the corresponding positions is not higher than in the surroundings (data not shown). From Fig. 14, the flow path lines coming from upstream in the counterflow region exhibit a flow pattern that diverts the counterflow region either upward or downward and that shrinks toward the equatorial plane direction from the periphery starting over halfway across the counterflow region.

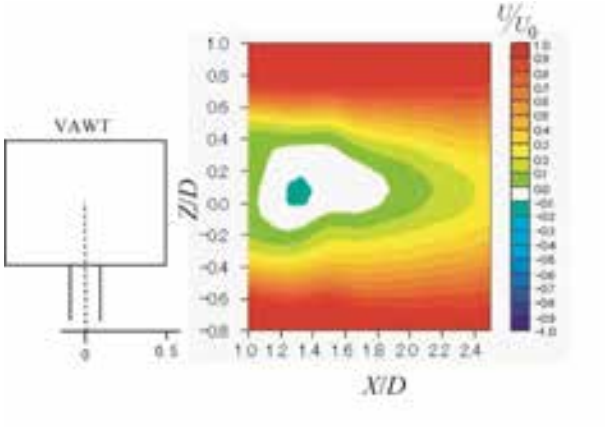

Fig. 13 Distribution of velocity component *U* on vertical plane of *Y/D* = 0.5

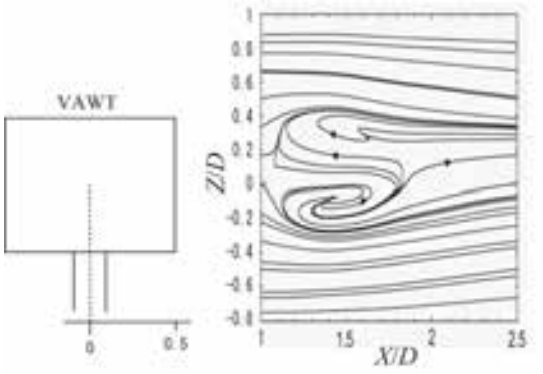

Fig. 14 Two-dimensional path lines on vertical plane of *Y/D* = 0.5

Figure 15 shows the two-dimensional flow path lines in the *Y-Z* plane perpendicular to the main flow at position *X/D* = 1.33. From Fig. 15, relatively large secondary flows occur from the vertical direction toward the equatorial plane at the rotor center and on the left side as viewed from downstream, and a flow occurs from left to right near the equatorial plane. In the wake area of the rotor right edge (*Y/D* = 0.5), the flow path lines converge at two points above and below, showing that a complex flow field is formed.

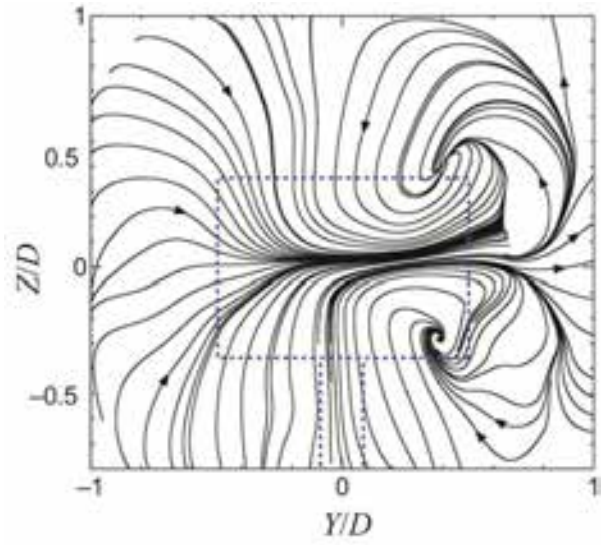

Fig. 15 Two-dimensional path lines on vertical plane of *X/D* = 1.33

As shown earlier, the averaged flow field exhibits an extremely complex flow state near the counterflow region, and the state of the flow field cannot be understood sufficiently well by examining only the flow patterns in two-dimensional cross sections in each direction. Calculations of the three-dimensional flow path lines of the average flow field were therefore performed taking several specific locations as the initial positions. An example of the results is shown in Fig. 16, which shows the trajectories of 6 test particles for which the initial positions were all on the equatorial plane (*Z/D* = 0) at *X/D* = 1 with *Y* coordinates *Y/D* = 0.4 for particle 1, *Y/D* = 0.25 for particle 2, *Y/D* = 0.1 for particle 3, *Y/D* = 0 for particle 4, *Y/D* = -0.25 for particle 5, and *Y/D* = -0.4 for particle 6. After starting, particle 1 first moved below the equatorial plane temporarily before returning to the vicinity of the equatorial plane again, and then returned to become only slightly upstream while moving in the +*Y* direction and then flowing downstream. Particles 2 and 3 had trajectories that traced out a single loop near the equatorial plane, and then after returning toward the upstream direction they flowed downward below the equatorial plane before flowing toward the outside while approaching the equatorial plane again. Particle 4 traced out a relatively large semicircular trajectory near the equatorial plane before returning upstream, and then

flowed downstream while shifting considerably in the +*Z* direction, and then after reaching a height near the top edge of the rotor it flowed generally along the main flow direction. Particles 5 and 6 flowed from the -*Y* side toward the +*Y* side while shifting slightly toward the +*Z* direction, and particle 6 in particular accelerated in the downstream direction.

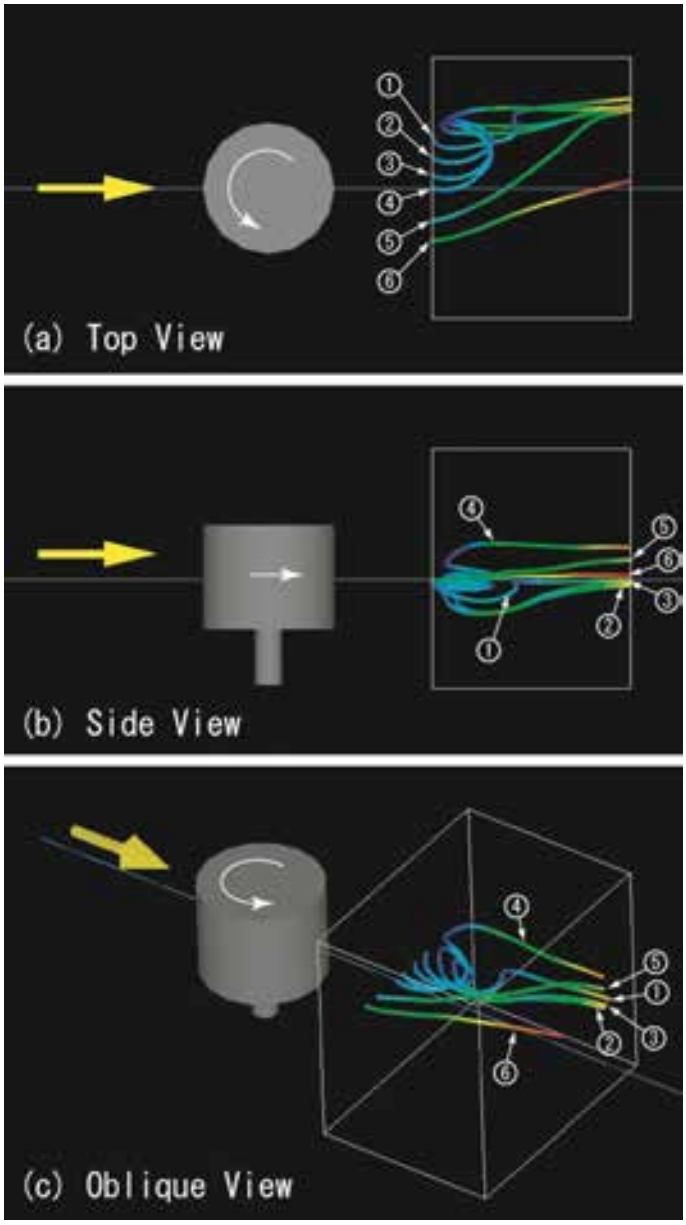

Fig. 16 Three-dimensional path lines in wake of VAWT

Conclusion

The counterflow region observed in the averaged flow field of VAWT wake was shown to have been formed by a vortex-shaped flow pattern. Furthermore, details of the complicated averaged flow field in the vicinity of the counterflow region were determined by calculation of three-dimensional flow path lines. Problems remaining for the future are finding the averaged dynamic flow field by other methods such as CFD in order to investigate whether the same averaged flow field can be obtained as in this research, and finding the three-dimensional velocity fields near the rotor and inside the rotor.

Acknowledgements

The experiments in this research were conducted at the large wind tunnel facility installed at Tottori University with support from scientific research funds for 2000 to 2002 (Grant-in-Aid for University and Society Collaboration; Representative: Tsutomu Hayashi).

References

[1] I. Paraschivoiu. *Wind Turbine Design with Emphasis on Darrieus Concept.* Polytechnic International Press, pp. 147-264, 2002.

[2] M. O. L. Hansen. *Aerodynamics of Wind Turbines*. James & James, pp. 48-59, 2000.

[3] D. A. Spera (ed.). *Wind Turbine Technology*. ASME Press, pp. 215-282, 1994.

[4] V. Kumar, M. Paraschivoiu and I. Paraschivoiu. Low Reynolds Number Vertical Axis Wind Turbine for Mars. *Wind Engineering*, Vol. 34(4), pp. 461-476, 2010.

[5] Y. Hara, T. Suzuki, Y. Ochiai and T. Hayashi. Measurements of the Wake of a Small Straight-Bladed Vertical Axis Wind Turbine. *Proceedings of the JSME Fluids Engineering Conference 2010*, No.10-16, pp. 429-430, 2010, (in Japanese).

[6] Y. Hara, T. Suzuki, Y. Ochiai and T. Hayashi. Measurements of the Wake of Small Vertical Axis Wind Turbine by Using an Ultrasonic Anemometer. *Proceedings of the 49th General Assembly and Conference of the Chugoku-Shikoku Section of the JSME*, No. 115-1, pp. 383-384, 2011, (in Japanese).

[7] Y. Hara, T. Suzuki, Y. Ochiai and T. Hayashi. Velocity Field Measurements in Wake of a Straight-Bladed Vertical Axis Wind Turbine. *Proceedings of ASME-JSME-KSME Joint Fluids Engineering Conference 2011*, AJK2011-07002, 2011.